ADVANCED MULTIPOLES AND APPROPRIATED MEASUREMENT TOOLS FOR FIELD CHARACTERIZATION OF SIS100 MAGNETS

Pierre Schnizer, Anna Mierau, Anke Gottsmann, Florian Kaether, Harald G. Weiss
Egbert Fischer, GSI, Darmstadt, Germany
Bernhard Schnizer, TU-Graz, Graz, Austria

Abstract

The heavy ion synchrotron SIS100 utilises fast ramped superconducting magnets. Describing and measuring these magnets requires advanced multipoles next to well adapted measurement techniques. We cover briefly the required theory adapted to the measurements, show which designs were available and which decisions had to be taken for measuring curved superconducting magnets. The series of SIS100 dipole magnets is going to be produced. These magnets will be measured at GSI. We present the foreseen field measurement procedure, outline the currently ongoing tests and give our calibration strategy.

INTRODUCTION

The heavy ion synchrotron SIS100 utilises fast ramped superconducting magnets [1, 2]; in particular as the vacuum chambers' inner surface is used as adsorption pump and thus has to be cold [3, 4].

These requirements led to a curved dipole with minimised aperture. The field provided within the aperture gap has to be fully understood so that today one can already forecast if the magnet's field quality will support the project targets of the high current machine.

The development of the advanced multipoles [5–7] allows describing the field within the curved beam path and the elliptic cross section of the vacuum chamber.

The required measurement devices were prepared in parallel adapted to the theoretical limitations.

THEORY

The standard description of the magnetic field for accelerator magnets is given by

$$B_y + \mathrm{i}B_x = \mathbf{B(z)} = \sum_{n=1}^{\infty} \mathbf{C_n} \left(\frac{\mathbf{z}}{R_{Ref}} \right)^{n-1} \qquad (1)$$

with $\mathbf{B}$ the 2D magnetic field and $\mathbf{C_n}$ the coefficient n, $z = x + \mathrm{i}y$ and R_{Ref} the reference radius. For elliptic apertures elliptic coordinates are adapted to the geometry. These coordinates (e.g. [8]) are given by

$$x + \mathrm{i}y = \mathbf{z} = e \cosh(\mathbf{w}) = e \cosh(\eta + \mathrm{i}\psi), \qquad (2)$$

with x and y the Cartesian 2D coordinates, and $e = \sqrt{a^2 - b^2}$ the ellipse eccentricity. Then the field is given by

$$\mathbf{B(w)} = \frac{\mathbf{E_0}}{2} + \sum_{m=1}^{\infty} \mathbf{E_m} \frac{\cosh(m\mathbf{w})}{\cosh(m\eta_0)}, \qquad (3)$$

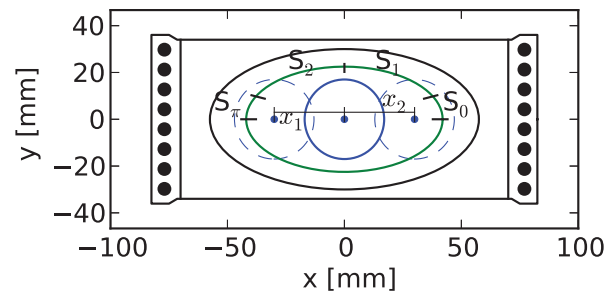with $\mathbf{E}_m$ the elliptic coefficients and $\eta_0 = \tanh^{-1}(b/a)$.

Figure 1: Rotating coil probe positions for measuring elliptic multipole coefficients. The beam aperture is indicated by a black ellipse. The green ellipse indicates the ellipse used currently in reconstruction. The blue circles indicate the area covered by the coil probe. S_0, S_1, S_2, S_π indicate the different parts where the coil probe is used. x_1 gives the offset of the coil probe measurement from the centre to the left side while x_2 gives the offset of the coil probe form the measurement to the right side. The magnet turns are indicated by the black filled circles and its inner aperture by a line.

Deduction of Equations for Error Analysis

The elliptic multipoles are derived from measurements from different positions (see Fig. 2) [5]. The coefficients $\mathbf{E_m}$ are obtained using the Fourier cosine transform

$$\mathbf{E}_m = \frac{2}{\pi} \int_0^\pi \mathbf{B}(\eta_0 + \mathrm{i}\psi) \cos([m]\psi) \, \mathrm{d}\psi, \qquad (4)$$

with $\mathbf{B}$ the magnetic field along the ellipse, ψ the angle along the ellipse. The reconstruction is split in three parts for each coil, which finally add up to six parts as the parts which intermix have to be taken into account.

The coefficients were calculated numerically as given in [5]. An equivalent analytic expression is given below which allows deriving the influence of measurement errors.

All three coil probes will measure the same field described by some coefficients $\mathbf{C_n}$. While the coefficients obtained by the central coil probe are the $\mathbf{C_n}$, the ones obtained by the translated ones are given by

$$\mathbf{C'_n} = \left[\mathcal{L} \binom{n-1}{k-1} \left(\frac{\mathbf{d_z}}{R_{Ref}} \right)^{n-k} \right] \mathbf{C_k}. \qquad (5)$$

$\mathcal{L}$ indicates that this expression is an upper triangular matrix. This expression represents the so called "feed-down effect". On these set of harmonics ($\mathbf{C'^r_n}$ for the coil on the right, $\mathbf{C'^c_n}$

for the coil in the centre, $\mathbf{C}^{l'}_n$ for the coil on the left) the various artefacts are applied. Then these are transformed back so that $\mathbf{C}^r_n$, $\mathbf{C}^c_n$ $\mathbf{C}^{l'}n$ are valid at the centre. These are transformed to coefficients of elliptic multipoles using [5]

$$\mathbf{E}_k = \sum_{m=k}^{M} \mathbf{C}_m \alpha^{m-1} \left[\frac{1}{2}\right]^{m-2} ((m+k+1) \bmod 2) \binom{m-1}{\frac{(m-k)}{2}}, \tag{6}$$

with $\alpha = e/R_{Ref}$.

The field is reconstructed using the appropriate coil probe data, the parts $S_0 \ldots S_\pi$ (Fig. 2) are selected with the function unitbox U

$$U(x) = H(x^2 - 1/4) \tag{7}$$

with H, the Heaviside step function. For the range $0 \ldots \pi$ the different parts are given by

$$S_0(\psi) = \frac{\psi}{2\psi_c}, \qquad S_1(\psi) = -\frac{2\psi_c - 4\psi + \pi}{2\pi - 4\psi_c}, \tag{8}$$

$$S_\pi(\psi) = \frac{\psi - \pi}{2\psi_c} \quad \text{and} \quad S_2(\psi) = \frac{-2\psi_c - 4\psi + 3\pi}{2\pi - 4\psi_c}. \tag{9}$$

In the parts S_1 and S_2 the left or right measurement data are mixed with the central data. These are mixed by a smoothing function

$$P(p) = 3p^2 - 2p^3. \tag{10}$$

Using the expressions above the field combinations $\mathbf{B}_p$ are given by

$$\begin{aligned}\mathbf{B}_p(\psi) = & \left(\left[U(S_0)) + \tfrac{1}{2}U(S_1)(1 - P(S_1 + \tfrac{1}{2}))\right] \mathbf{E}^r_m \right. \\ & + \left[\tfrac{1}{2}U(S_1)(P(S_1 + \tfrac{1}{2})) + \right. \\ & \left. + \tfrac{1}{2}U(S_2)(P(S_2 + \tfrac{1}{2}))\right]\mathbf{E}^c_m \\ & \left. + \left[U(S_\pi)) + \tfrac{1}{2}U(S_2)(1 - P(S_2 + \tfrac{1}{2}))\right] \mathbf{E}^l_m\right).\end{aligned}$$

S_0, S_1, S_2 and S_π are functions of ψ. Using (3) and (11) (4) can be expressed by

$$\mathbf{E}_m = \frac{2}{\pi} \frac{1}{\cosh(m\eta_0)} \int_0^\pi \mathbf{B}_p \, \cosh(m[\eta_0 + \mathrm{i}\psi]) \mathrm{d}\psi. \tag{11}$$

These expressions allow studying the influence of the measurement artefacts of the individual measurement on the finally obtained field harmonics.

Influence of Coil Displacement

As illustration uncertainties of x_1 or x_2 are studied. For these calculations $x_1 = -x_m + \Delta z$ is used in the transformation of $\mathbf{C}^l$ to $\mathbf{C}^{l'}$. Similarly $x_2 = x_m + \Delta z$ is used for $\mathbf{C}^r \rightarrow \mathbf{C}^{r'}$. These are then transformed back to the coordinate system at the origin by using $x_1 = x_m$ and $x_2 = x_m$. The obtained multipoles are then transformed to the equivalent elliptic multipoles using (11). The multipoles $\mathbf{E}^l_m$, $\mathbf{E}^c_m$, and $\mathbf{E}^r_m$ are then inserted in (11) and (11).

For describing the artefacts the following expressions are introduced:

$$\mathcal{L}_e = \mathbf{C}_{m-1}\alpha^{m-2}\left[\frac{1}{2}\right]^{m-3}((m+n) \bmod 2)\binom{m-2}{\frac{m-n+1}{2}} \tag{12}$$

and

$$\mathcal{L}_{dz} = \frac{m-n}{m}\binom{m-1}{n-1}\mathbf{dzs}^{m-n-1}, \tag{13}$$

with $\mathbf{dzs} = \mathbf{dz}/R_{Ref}$. The first one transforms the circular to elliptic multipoles while the second one is similar to the feed-down effect. The angle ψ where the measurement circle intersects the ellipse is denoted with ψ_c. Then further $\xi = (\pi - 2\psi_c)$ is introduced.

The artefacts of the elliptic harmonics E_m share a constant factor

$$\begin{aligned}t_f = & \left(m^4\xi^3\left[2\psi_c + \pi\right] + 24\right)\cosh(m\eta) + \\ & 24\cosh\left(m\left[\eta - 2\mathrm{i}\psi_c\right]\right) - \\ & -2\mathrm{i}m\xi\{\left(m^2\xi^2 - 6\right)\sinh(m\eta) + \\ & 6\sinh\left(m\left[\eta - 2\mathrm{i}\psi_c\right]\right)\}\end{aligned} \tag{14}$$

for the odd harmonics. For even harmonics a factor

$$t_f^e = -24\left(2\cosh(m\eta) + im\xi\sinh(m\eta)\right) \tag{15}$$

has to be added to t_f. So the spurious harmonics due to a shift $\mathbf{dzs}$ of one of the coils are given by

$$\mathbf{E}_m = \left[\frac{1}{4m\pi}\mathcal{L}_e * \mathcal{L}_{dz}\left(t_f[1 + (m+1 \bmod 2)]t_f^e\right)\right] q\,\mathbf{C}_n. \tag{16}$$

The "*" denotes a element wise multiplication. q is 1 for the coil on the right and -1 for the coil on the left. These results are preliminary and the relevant conclusions to be drawn.

SERIES MEASUREMENT SYSTEM

Different prototype magnets were built and measured [9–11] using rotating coil probes. These verified the necessity to cover as much of the beam aperture as possible to gain reliable field coefficients. Therefore different measurement system options were evaluated for the measurement campaign for the series magnets:

- a curved rectangular anticryostat for accessing the magnet's aperture, and rotating coil probes for measuring the magnet's field,

- a straight circular anticryostat in the magnet gap and rotating coil probes for field measurement,

- or cold rotating coil probes operated in vacuum.

(see also Fig 2). It is common to all these options, that the coil probes have to be relocated transversally. This movement can be made when an anticryostat is used; for the cold coil probes, due to the support systems of the bearings it can be only made with the foreseen ball bearing supports when the magnet is warmed up and cooled down again.

The anticryostat options and in particular the rectangular anticryostat were thoroughly investigated. These anticryostats have to sustain ambient pressure inside and vacuum pressure on the outside. A rectangular anticryostat, which can be built using today's technology reduced the
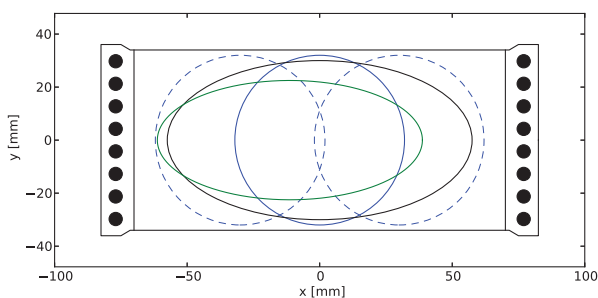
Figure 2: Area covered by the different measurement methods. The black ellipse indicates the beam aperture. The blue circles indicate the measurement area of the cold coil probes (solid: centre, dashed: left and right). The green ellipse indicates which area can be covered if a straight anticryostat and coil probes at warm are used.

aperture significantly so that this option was not further investigated.

At GSI a round anticryostat exists which can be translated horizontally using the moveable tables at the ends. It also gives only access to a limited aperture; further it is mechanically only of limited stiffness and thus the coil probe transversal position can be reached only with an accuracy of up to a few millimeters.

The cold coil probe, however, covers even at is centre position a circle with a radius of 32 mm. The round anticryostat only allows covering an ellipse with half axes a =45 mm and b =22.5 mm, with a and b the half axes of the ellipse. The rectangular anticryostat provided an area so that the biggest ellipse inside was a =45 mm and b =22.5 mm.

All these circumstances led to test a cold rotating coil probe in vacuum [12], which was lent by CERN. Here a rotating coil probe is inserted within the magnet aperture. The signals and torque are transmitted from outside by a vacuum feed through. As this test was successful, this path was pursued.

SHAFT DEVELOPMENT

A mockup of the shaft has been implemented. Due to the machine's radius and a sensible coil length of ≈ 600 mm, the bellows between the coils have to provide a longitudinal play of several milli-radians while the overall torsional stiffness of the shaft shall be kept below ≈ 0.1 milli-radians. Tests of the first bellows showed that these can provide the longitudinal play and do not introduce any significant vibrations into the shaft. The torsional stiffness is currently under investigation but already close to the target. In next step the mock up will be tested within the universal cryostat to see that it provides the same behaviour as at room temperature. Currently the coil mock ups are made of PVC while the coil probes bodies will be made of G11, which will further improve the stiffness of the assembly.

CALIBRATION STRATEGY

Up to four test benches will be available for measuring dipoles [12]. The cold coil probe method demands several sets, as these have to rest within the magnet during the whole testing period. Thus different shafts will be used for measuring different magnets. Therefore diligence must be devoted to the calibration of the different shafts. The following strategy is foreseen:

- the coil probes will be calibrated as a shaft in a dipole field at room temperature,

- the contraction is of the order of 10^{-3} and thus has only to be known with an accuracy of a few percent.

- the integrators will be recalibrated using a precise voltage source and frequency generator,

- and finally cross check measurements will be made with a single stretched wire.

CONCLUSION

The theory and measurement systems are being prepared for the SIS100 dipole magnets. The field coefficients are obtained from three rotating coil probe measurements. The combination method has been established and is at use at GSI for several years now. An adequate formulation for error propagation analysis has been presented.

The shaft for the series measurement is in preparation with a mockup already built and tested. An adequate calibration strategy was discussed.

REFERENCES

[1] E. Fischer et al. "The SIS100 superconducting fast ramped dipole magnet" IPAC'14, Dresden, June, 2014, WEPRI083, (2014), http://www.JACoW.org

[2] E. Fischer et al., IEEE T. Appl. Supercon. 4003805 (2014)

[3] S. Wilfert and K. Keutel, Die kryogenen Vakuumkammern der supraleitenden Magnete der SchwerIonenSynchrotron-Ringe SIS 100/300. Technical report, Otto-von-Guericke-Universität, 2004.

[4] E. Fischer et al., "SIS100 fast ramped magnets and their cryopump functionality for the operation with high intensity intermediate charge state heavy ions" IPAC'10, Kyoto, May 2010, MOPEB025, (2010).

[5] P. Schnizer et al., NIMA 607(3):505– 516, (2009).

[6] P. Schnizer et al., "Theoretical Field Analysis for Superferric Accelerator Magnets Using Elliptic Multipoles and its Advantages", EPAC'08, Genova, WEPD021, June 2008.

[7] P. Schnizer, B. Schnizer, and E. Fischer, "Cylindrical circular and elliptical, toroidal circular and elliptical multipoles, fields, potentials and their measurement for accelerator magnet", arXiv preprint physics.acc-ph, October 2014.

[8] P. Moon and D. E. Spencer. *Field theory handbook* (Springer, 1988).

[9] E. Fischer et al., "Measured and calculated field properties of the SIS100 magnets described using elliptic and toroidal multipoles" PAC'09, Vancouver, May 2009, TH5PFP057 (2009).

[10] E. Fischer et al. EEE T. Appl. Supercon, 20(3):218–221 (2010).

[11] P. Schnizer et al. "Commissioning of the mole for measuring SIS100 magnets and first test results" IEEE T. Appl. Supercon, 20(3):1977–1980 (2010).

[12] P. Schnizer et al, IEEE T. Appl. Supercon., 9500505 (2014).